PEDESTRIAN CRASH RECONSTRUCTION USING MULTI-BODY MODELING WITH GEOMETRICALLY DETAILED, VALIDATED VEHICLE MODELS AND ADVANCED PEDESTRIAN INJURY CRITERIA

Lex van Rooij, Kavi Bhalla, Mark Meissner, Johan Ivarsson, Jeff Crandall
University of Virginia, USA
Douglas Longhitano
Honda R&D Americas, Inc., USA
Yukou Takahashi, Yasuhiro Dokko, Yuji Kikuchi
Honda R&D Co., Ltd., Japan
Paper Number 468

ABSTRACT

This paper develops a method for studying pedestrian to car impacts through detailed multi-body modeling of various pedestrian anthropometries and vehicle types. The pedestrian models constitute a multi-body representation of the global joint kinematics and inertia for five representative body sizes. Advanced injury criteria are defined for the pedestrian lower extremities, knee, thorax and head. The vehicle model of a small family car is defined by a facet element mesh for the front-end and windshield of the car. The contact stiffness is variable over the location on the vehicle mesh and has been validated against experimental results and FE simulations of the EEVC impactor tests. The underlying structures of the hood are defined as rigid ellipsoids. The developed model is applied to the reconstruction of two PCDS cases with a small family car. Injury risk data was collected from the simulation model and compared to the injury outcome for the pedestrians involved in these two cases. Results of this study show that the detailed model can distinguish the injury severity for various body parts at impact locations on the vehicle.

INTRODUCTION

Pedestrian fatalities in the US reached 4,882 in the year 2001, while 78,000 people were injured in pedestrian to vehicle crashes (NHTSA 2001). This represents 12.9% of the total traffic fatalities and 3.9% of all injuries in traffic in that year. While pedestrian fatalities in the US have decreased by 16% since 1991, due to better education, smoother designs for improved aerodynamics and safer infrastructure, the vulnerable road user problem has grown larger on a global scale. Mackay (2000) estimates the total amount of traffic fatalities worldwide at 950,000 in the year 2000, while the World Bank (2003) states that 65% of all traffic fatalities involve pedestrians. Therefore, the total number of yearly worldwide pedestrian traffic fatalities is as high as 615,000.

More than 50% of all pedestrian injuries are caused by an interaction with the front of the vehicle as Figure 1 shows (Otte 2001). The bumper area generally causes lower extremity injuries, the hood edge area causes hip and abdominal injuries, while contact with the hood and windshield accounts for injuries to thorax, head and neck. Impacts to these vehicle areas are the focus of this paper, while the remaining injuries caused by an impact to the road or to any other undefined object are not investigated.

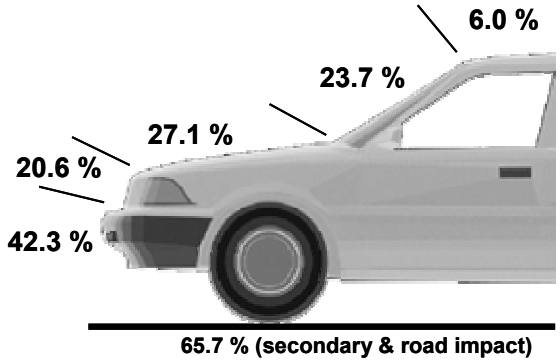

Figure 1. Injuries sustained to pedestrians per vehicle region (Otte 2001).

The injury distribution per body region denoted in Figure 2 clearly shows that most severe and life threatening injuries (AIS 5-6) are sustained to the head, followed by thorax, abdomen and spine. Less severe injuries (AIS 2-4) are in 37% of the cases sustained to the lower extremities and pelvis, while the head accounts for 35% and the torso and upper extremities for the remaining 28%. This illustrates the importance of focusing on injuries to lower extremities and head, and to a lesser degree to injuries to the thorax, abdomen, spine and upper extremities.

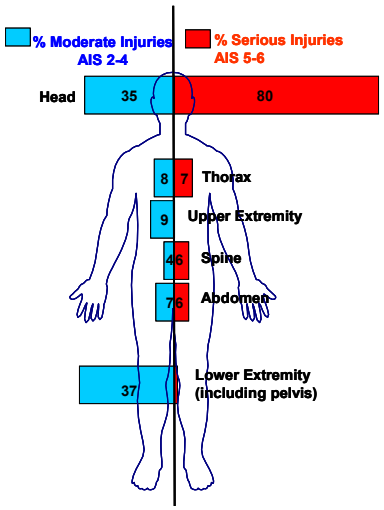

Figure 2. Pedestrian injury distribution per body region (Chidester 2001).

The pedestrian population extends from toddlers to the elderly population. Results published by NHSTA (NHTSA 2001) from the Fatality Analysis Reporting System (FARS) and from the National Automotive Sampling System General Estimates System (GES) demonstrate that pedestrians of all age groups are at risk. Figure 3 shows that people 25 years and older account for 78.7% of all pedestrian fatalities. It also shows that 39.7% of the injured pedestrian population are 20 years or younger. Therefore, we can conclude that middle aged and elderly people are more likely to die in a pedestrian crash, while younger people and children are more likely to be injured in a pedestrian impact.

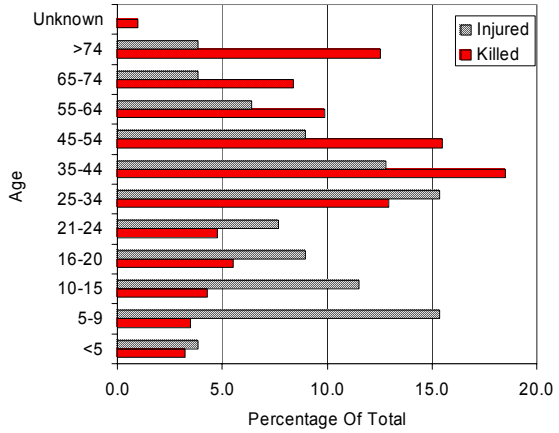

Figure 3. Pedestrian injury and fatality ratios per age group (NHTSA 2001).

Previous research in pedestrian safety includes accident reconstruction, the development of mathematical and experimental human pedestrian surrogates and biomechanical research of the mechanical behavior of anatomical structures in response to impact loading. The US government conducted the Pedestrian Injury Causation Study (PICS) in the late 1970s, where data was recorded from the accident scene, the case vehicle and the medical reports (Jarrett 1998). In the 1990s the Pedestrian Crash Data Study (PCDS) was initiated in response to a modernized vehicle fleet. The PCDS database contains detailed reports on reconstructions of the crash. Data is recorded and analyzed based on the accident scene, the status of the case vehicle, medical records, police reports and interviews with people involved in the crash and with possible witnesses (Chidester 2001). From an in-depth analysis of real-world pedestrian to vehicle crashes it is possible to obtain a better understanding of the mechanisms that cause injury.

The European Enhanced Vehicle-Safety Committee (EEVC) Working Group 10 recognized the need for regulations in the design of the front structure of passenger vehicles and developed a standardized test method to evaluate this (EEVC 1994). EEVC Working Group 17 evaluated the previously developed test methods and proposed improvements to the test method based on new data from accident investigations, biomechanical research and experimental tests (EEVC 1998). Experimental test devices have been developed that represent the head, the thigh and the full lower extremity as Figure 4 shows.

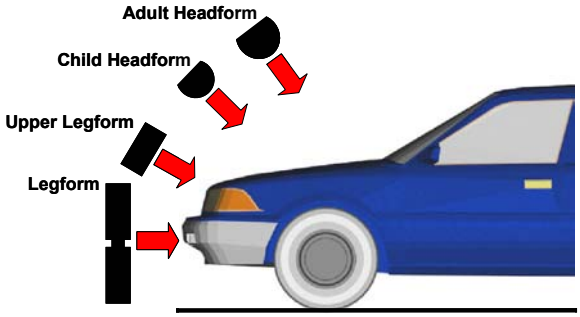

Figure 4. EEVC WG17 pedestrian impactor subsystems.

The headform impactor is a rigid device in free flight and records linear acceleration upon impact with the hood with a prescribed speed of 40 km/h and an angle of 65º with the ground reference level for the adult headform and 50º for the child headform. No test of a headform with the windshield is required. The upper legform impactor is designed to test the hood edge of a vehicle. The impact energy and angle are dependent on the geometry of the front of the vehicle. The legform impactor represents a thigh and a leg and has a deformable knee joint, where bending

angle and knee shear are recorded. An impact with the bumper at 40 km/h is prescribed in the requirements.

A beneficial alternative to experimental testing is mathematical modeling of pedestrian to vehicle impact. Computational simulation is often cost and time efficient and the influence of varying conditions can easily be investigated. Mathematical modeling of pedestrian impact was initiated with an investigation of the biofidelity of multi-body human models with 2 to 15 segments (Wijk 1983). These models were compared to pedestrian dummy tests. Later mathematical studies involved a 15 segment model developed from the GEBOD anthropometric database (Ishikawa 1993, Yang 2000). Joint characteristics are implemented based on biomechanical data from cadaveric tests. The models have been validated against full scale cadaveric impact tests with the fronts of various vehicles. In a parametric study the formerly discussed 15 segment human model is combined with multi-body models of four different types of vehicles, consisting of one ellipsoid for bumper, one for the hood leading edge, one for the hood and one for the windshield (Yang 2000). It is concluded that a reduction of impact speed from 40 km/h to 30 km/h and an increase of the hood height have a positive influence on the head injury risk, while the knee joint injury severity is mainly influenced by bumper height and stiffness (Liu 2002a). Five child anthropometries are scaled from this model and stiffness properties are based on the age dependency of dimensions of anatomical structures and of material properties (Liu 2002b). In child pedestrian impact a reduction of impact speed from 40 km/h to 30 km/h is shown to have a great influence on the injury severity, while vehicle design parameters show conflicting effects due to the variability in child anthropometry (Liu 2002c).

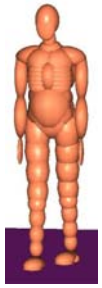

Figure 5. MADYMO 50th percentile male human pedestrian model.

MADYMO developed a 50th percentile human male pedestrian model, consisting of 52 segments and stiffness and fracture behavior based on biomechanical data (TNO 2001a). Scaling methods allow the user to define any desired anthropometry. Validation of this model is performed against 8 full body cadaveric pedestrian to midsize sedan vehicle impacts and the model has been applied to reconstruct a fatal crash (Coley and de Lange 2001). Bhalla (2002) investigated the performance of the MADYMO human pedestrian model in throw distance prediction and compared this to existing throw distance formulas and accident reconstruction software. The vehicle front geometry and contact stiffness appear to have a great influence on the resulting throw distance, while it is concluded that the MADYMO human pedestrian model needs further validation for the use of throw distance prediction. Due to the complex behavior of the human lower extremity and increasing computational capacity, finite element (FE) models of the lower extremity in pedestrian impact are being developed (Schuster 2000, Takahashi 2000, Maeno 2001). All models consist of a detailed geometry of bone, cartilage, ligaments and flesh of the lower extremity. Constitutive material models are implemented based on biomechanical experiments on cadaveric lower limbs. The models are coupled to full human body models and validated against component and full scale cadaveric tests. In the future, other areas of the human body will be implemented in FE to serve as a detailed tool to study the injury mechanisms occurring in pedestrian to vehicle impact.

Summarizing, pedestrian crash reconstruction databases provide valuable information on the mechanisms that cause injury, the EEVC WG17 test procedure is a reasonably objective procedure to evaluate the pedestrian safety of various components of a vehicle, while mathematical multi-body human models provide a biofidelic predictor of the kinematics and injury risk in a pedestrian to vehicle impact. The goal of this study is therefore to develop detailed multi-body vehicle models and to validate them against EEVC impactor tests. The acquired vehicle model is then applied together with the human model to evaluate two pedestrian crash reconstruction cases.

METHODS

Vehicle Model Development

The development of a detailed multi-body model of the case vehicle consists of the generation of the mesh of the front of the vehicle, building a multi-body framework of the vehicle and its suspension, characterizing the structures close under the vehicle surface and applying contact stiffness characteristics

to all areas of the vehicle where contact with a body part is suspected.

Facet Mesh Generation The case vehicle is a popular small family car. The mesh is obtained from a finite element model of the vehicle. First, the rear end of the vehicle is deleted. All elements behind the beginning of the roof, the a-pillar and the front fender can be deleted since contact of a pedestrian with those areas rarely occurs. Also, any structure underlying the outer surface of the vehicle is initially deleted, but is accounted for later. The final mesh contains great detail. For example, the edges of the grille were modeled in extremely small elements. All these very small elements are deleted for this application, since they will increase computational time and will not have an influence on the interaction with the human model. The resulting mesh consists of 20,829 nodes and 18,913 elements and as a result it accurately describes the outer geometry of the front of the vehicle, see Figure 6. The complete mesh is rigid, which allows for a computationally fast but nevertheless geometrically detailed contact stiffness description. The rigid mesh is in multi-body terminology often referred to as a facet mesh.

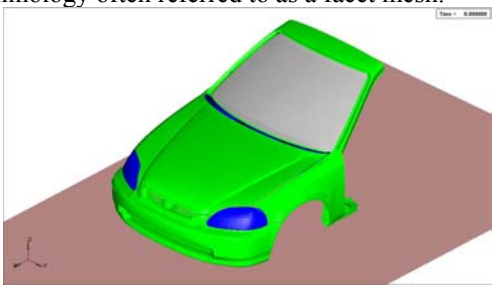

Figure 6. Facet mesh of the front of the case vehicle.

Multi-body Framework The chassis of the vehicle is represented by a relatively simple multi-body framework (Figure 7). The straightforward motion of the vehicle is prescribed by a one degree of freedom (DOF) translational joint, which connects the front tires to the road. The front axle with the unsuspended mass of the vehicle is represented by a rigid body that connects to the tires through a linear spring representing the stiffness of the two front tires.

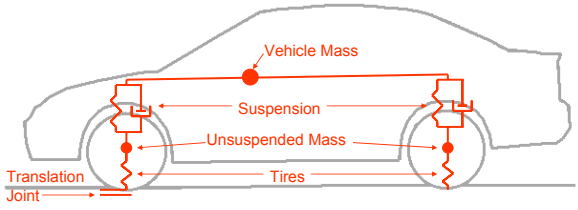

Figure 7. Multi-body framework with suspension model.

The suspended mass of the vehicle is connected to the front axle through a linear spring with a parallel damper element. The facet mesh is attached to this suspended mass. The connection to the rear axle with an unsuspended mass is also made by a linear spring with a damper element. The rear tires are represented by ellipsoids that are in contact with the road, with a contact characteristic representing the stiffness of the tires. The initial deflection of the suspension model is determined in a presimulation study with only gravity acting on the vehicle. To verify the suspension model, the resulting height of the chassis is compared to a real vehicle. Both axles are represented by joints with one rotational degree of freedom in the direction of the axle. As a result, the front and rear suspension work independently, allowing the car to pitch as a result of braking or an impact with a pedestrian.

Underlying Structures At various locations around the front of a vehicle a pedestrian will not only impact the outer structure, but will also strike structures underlying the outer surface. These structures tend to be very localized, especially within the engine compartment. As the pedestrian impacts the hood and the deflecting hood impacts the underlying structure, both structures cause a corresponding response on the body part that impacts.

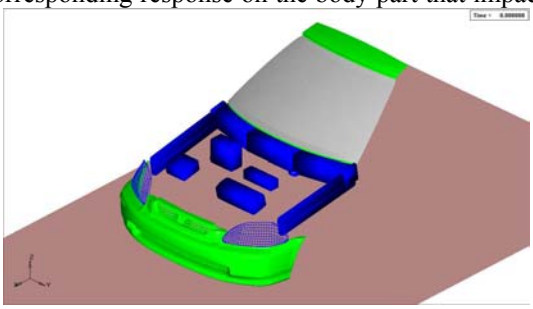

Figure 8. Vehicle model with defined underlying structures.

These structures are represented by multi-body ellipsoid descriptions and their locations are determined from either vehicle photographs or design drawings (Figure 8). The case vehicle contains two ellipsoids for the engine, one for the alternator, one for the battery and one for a control device near the cowl area. Furthermore, the case vehicle contains stiff areas at the cowl area and at the support of the hood at the fenders where additional ellipsoid structures were included.

Contact Stiffness Characterization The interaction of a pedestrian obviously depends heavily on the location of impact, since the compliance of the vehicle structure differs along the vehicle surface. In this study, important areas are identified and local

contact stiffness characteristics are defined. These contact characteristics were obtained from tests with EEVC impactors at prescribed impact conditions. Depending on the availability of test results, numerical FE simulations or experiments were used to provide acceleration history signals.

It is possible to define force-deflection contact stiffness characteristics based on acceleration history information, if the following requirements are met or assumed:

- The impactor is rigid and undeformable
- The total mass of the impactor is known
- The impactor is in free flight
- The impact direction is perpendicular to the surface
- The impactor does not rotate upon rebound from the surface

If these requirements are met or if they can be assumed the following equations convert acceleration a as a function of time t into force F and deflection x as a function of time:

$$F(t) = m \cdot a(t) \qquad (1).$$

$$x(t) = \int_0^t \left(\int_0^t a(t)dt \right) dt \qquad (2).$$

Then we are able to plot the force F as a function of deflection x (Figure 9). The contact stiffness curves are hence characterized by a loading curve with an elastic and a plastic part, and an unloading curve that defines the amount of hysteresis. This method will be followed for each area of the vehicle as discussed below.

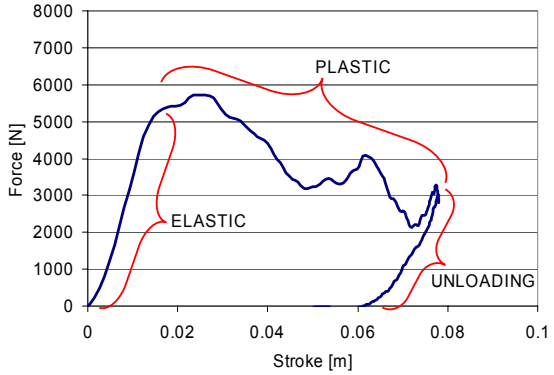

Figure 9. Typical contact force-deflection curve with elastic and plastic loading and unloading.

Windshield The windshield is generally known as a structure with a decreasing compliance closer to the center, away from the windshield frame (Mizuno 2000). Mizuno developed force-deformation characteristics from EEVC headform to windshield tests on a generic small family car at 40 km/h. Figure 10 shows four curves, measured from impacts with the windshield frame, 50 mm away from the frame, 150 mm away from the frame and in the windshield center. All curves are characterized by an initial spike of approximately 7.5 kN, which is caused by the fracturing windshield. After failure, a much lower stiffness occurs for all locations, which is caused by the stretching of the film layer that holds the broken glass together. Due to the varying stiffness curves as a function of the distance to the windshield frame, the windshield mesh of the model is subdivided in four similar regions (Figure 11).

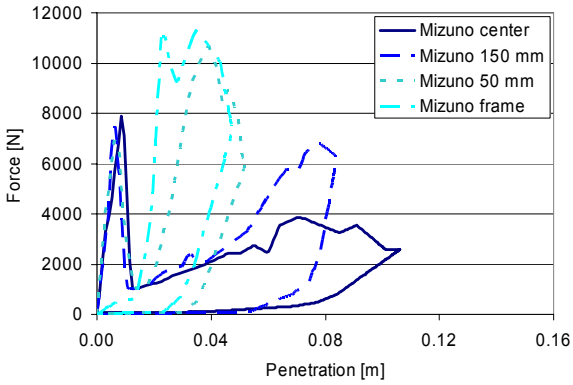

Figure 10. Force-deformation characteristics of 4 locations on the windshield as determined from EEVC headform impact tests (Mizuno 2000).

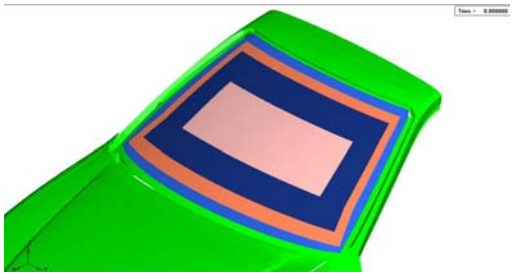

Figure 11. Four windshield regions; the windshield frame, 50 mm away from the frame, 150 mm away from the frame and the windshield center as defined for the model.

For the case vehicle, three EEVC headform impact tests have been performed. All three impacts were perpendicular to the windshield at 40 km/h. The acceleration history is denoted in Figure 12. The force-deformation curves were developed from the measured acceleration history and they are shown in Figure 13. One test was performed at the windshield center, while the other two were performed at locations approximately 100 mm away from the windshield frame, as Figure 14 shows.

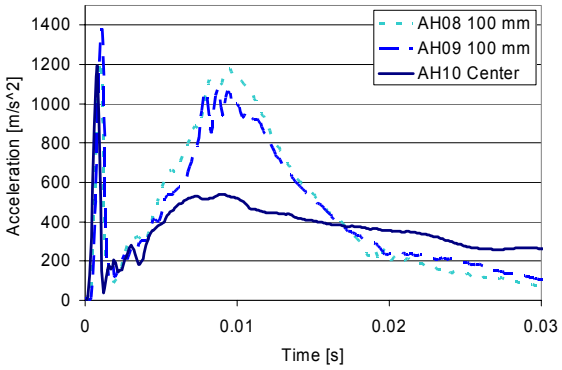

Figure 12. Acceleration history for three experimental EEVC headform impactor tests performed perpendicular to the windshield at 40 km/h.

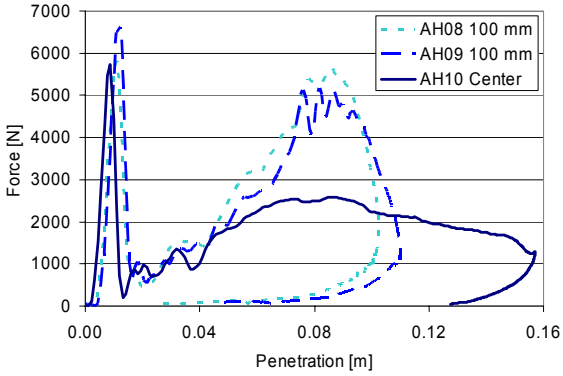

Figure 13. Force-penetration curves for three experimental EEVC headform impactor tests performed perpendicular to the windshield at 40 km/h.

Figure 14. Post-impact photographs of windshield impact locations for test AH10 (left) and AH08 (right).

The final force-deflection curves as applied to the model are defined as follows. 1) The stiffness for the center of the windshield is directly adopted from test AH10. 2) The stiffness for the areas 50 mm and 150 mm away from the windshield frame are based on the average of curves AH08 and AH09, both 100 mm away from the windshield, and are scaled for their respective distances to the windshield based on Mizuno's data. 3) The curve for the windshield frame stiffness is directly adopted from Mizuno's study, since no experimental test on the case vehicle is available. All the force-deflection curves of the model are shown in Figure 15.

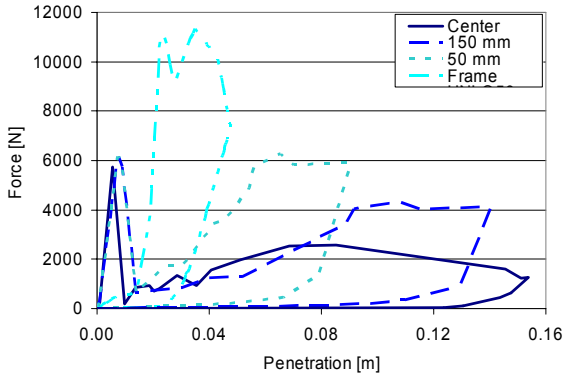

Figure 15. Force-deflection curves for the windshield at four different locations as defined for the model.

Finally, validation is performed and shown in Figure 16. The simulation of the impact with the center of the windshield compares very well with test AH10, while the curves for the simulations at 50 mm and 150 mm away from the windshield frame bracket the resulting curves of tests AH08 and AH09, as expected.

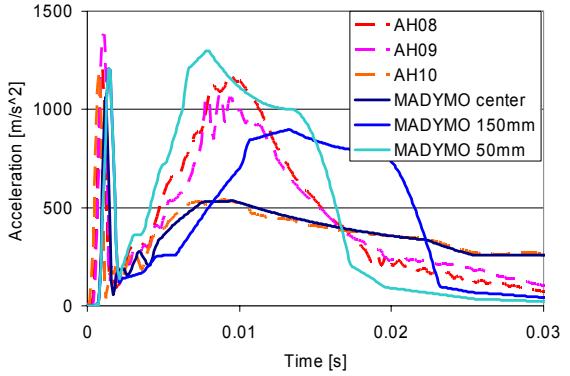

Figure 16. Validation of the windshield stiffness characteristic by comparing with the experimental tests.

A-pillar The a-pillar stiffness characteristic is defined from a single experimental headform impact test. The test is performed at an angle nearly perpendicular to the a-pillar. The a-pillar is not a flat structure and therefore, it can not be assumed that the impactor will rebound in the direction of impact without any rotation. As a result, it is impossible to develop a valid force-deformation curve from the measured acceleration history. Therefore, the unvalidated force-deformation curve is tuned by

performing iterative simulations of the headform impact until the acceleration history matches experimental results (Figure 17). The chosen characteristic is then validated by performing a simulation of the exact experiment. The result is shown in Figure 18.

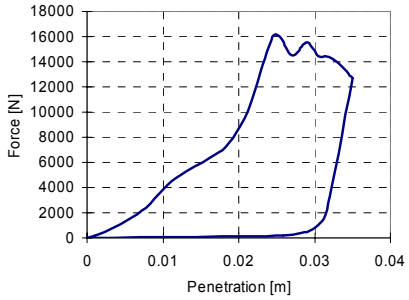

Figure 17. Force-penetraion curve for the a-pillar as adopted for the model.

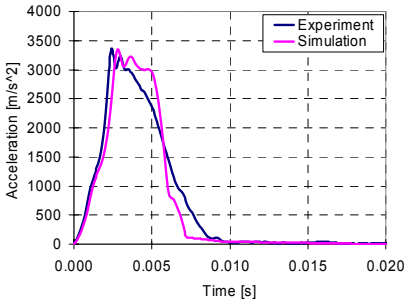

Figure 18. Comparison of experimental and computational acceleration history for headform to a-pillar impact.

Hood The hood is characterized as a uniform structure with one contact stiffness characteristic. A series of experiments are performed with an adult headform. The locations of impact to the hood are shown in Figure 19.

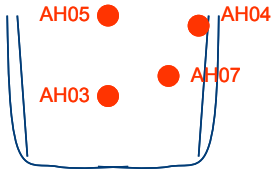

Figure 19. Experimental EEVC adult headform (AH) impactor test locations on the hood of the case vehicle model.

The resulting acceleration history curves are denoted in Figure 20. All tests are performed at EEVC requirements, except for the test denoted with 'AH03per', which represents perpendicular impacts. Most curves are characterized by an initial peak of approximately 130 g, after which an acceleration plateau comes in effect (Figure 20).

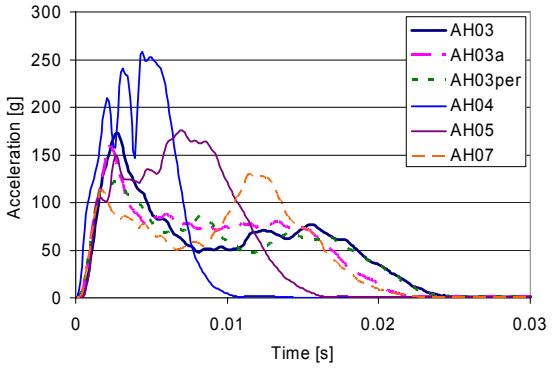

Figure 20. Experimental acceleration history curves from adult headform tests.

Test AH03per is a perpendicular test and it is a fair representative of the average hood stiffness. Therefore, this curve is converted into a force-deflection characteristic (Figure 21) and adopted for the model.

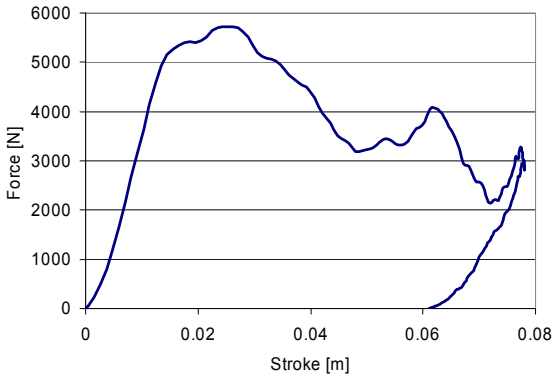

Figure 21. Force-deformation characteristic of the hood of the case vehicle.

Some curves show alternative behavior, which is caused by a structure underlying the hood that indirectly interacts with the headform. Test AH04 impacts the hood hinge and AH05 the cowl area, evident when comparing Figure 19 to Figure 8. Therefore, a contact interaction of the underlying ellipsoids with the head is defined as well. The linear stiffness constants are defined as 50 kN/m for the cowl and 97 kN/m for the hinges. The stiffness of the engine parts is defined as 200 kN/m, although this value can not be validated since there is no experiment where an impact with the engine occurs. Validation is then performed against all experimental headform impact tests. Figure 22 shows that test AH03 shows excellent resemblance. Test AH04 shows a similar peak, with a longer duration.

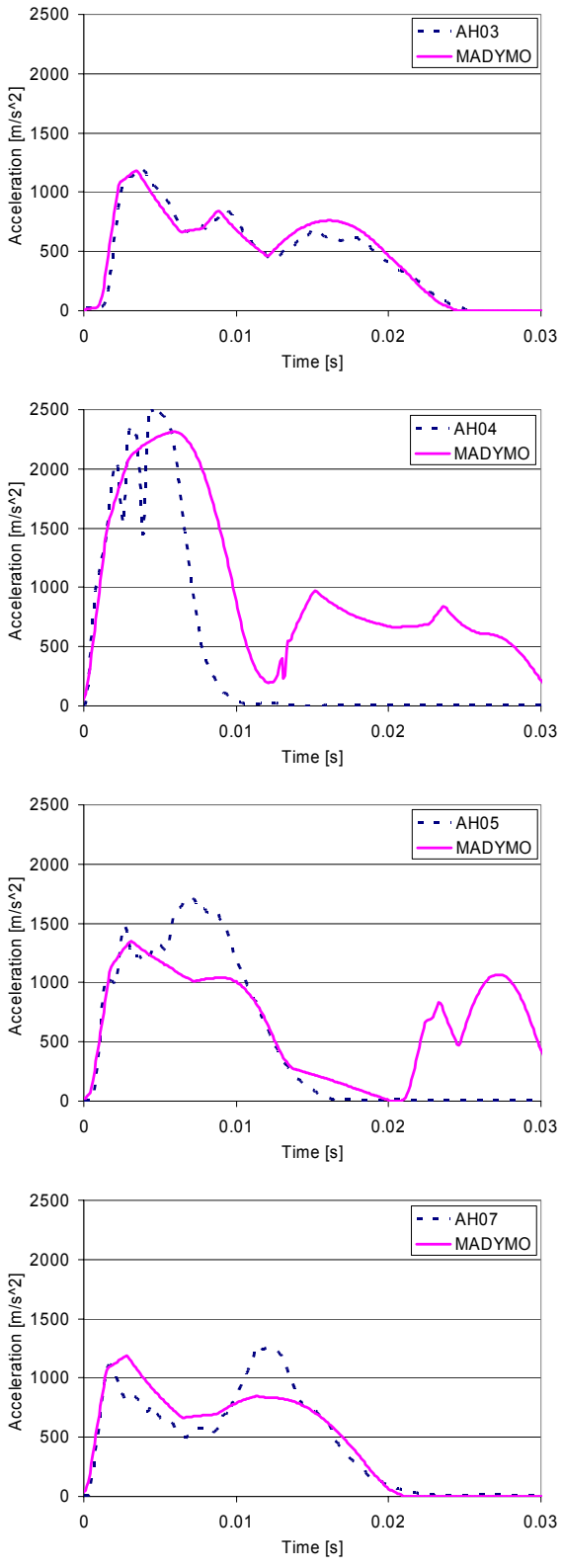

Figure 22. Acceleration history curves from experiments AH03, AH04, AH05 and AH07 and validation signals from MADYMO simulations.

Tests AH05 and AH07 show the correct initial peak, but the secondary peak can not totally be simulated. MADYMO Simulations of test AH04 and AH05 show a secondary acceleration pulse, which is caused by a secondary impact of the headform with the windshield. This is ignored for the validation.

Bumper The bumper area is one of the most important structures for pedestrian lower extremity protection. Compliance of a bumper shows a large gradient along the lateral axis of the vehicle. Figure 23 shows a schematic drawing of the front of the case vehicle, where three structurally different areas are observed. In the midsection, the compliance is determined by the bumper and the underlying bumper beam. The radiator-end area is characterized by again the bumper and the bumper beam and in addition the end of the radiator is supported relatively close to the bumper surface. This is expected to cause an increase in stiffness. The area where the side-frame connects to the bumper beam is structurally even stiffer.

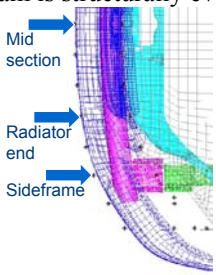

Figure 23. Schematic with a top view of the front of the case vehicles, where three structurally different areas are observed; midsection, radiator-end and side-frame.

Simulations are performed on an FE model of the case vehicle. A finite element model of the EEVC legform impactor is implemented as rigid and undeformable. The material properties of the foam are eliminated and the knee joint is locked. Impacts of the legform perpendicular to the bumper surface are performed at the three specified locations (Figure 24).

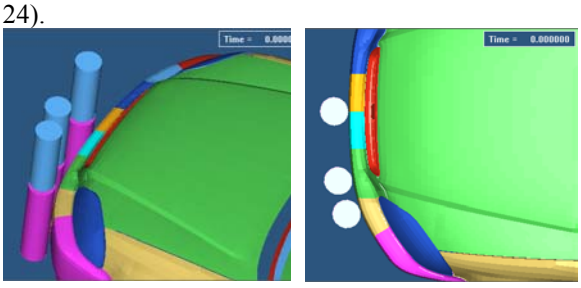

Figure 24. Test locations for legform to bumper simulations as performed on the FE model of the vehicle and on the final multi-body model for validation.

Results from the FE simulations are shown in Figure 25. The acceleration history is easily converted into a force-deformation plot, according to the method previously described. All curves are characterized by a low initial force plateau of approximately 3000 N caused by the compliance of the bumper itself. As the impactor penetrates deeper, other structures are contacted. Contact with the stiff bumper beam is characterized by a sudden increase in acceleration and force. The distance from bumper surface to bumper beam decreases moving away from the midsection along the lateral axis of the vehicle. Therefore, the steep rise occurs at lower penetration depths for radiator-end and side-frame compared to the midsection.

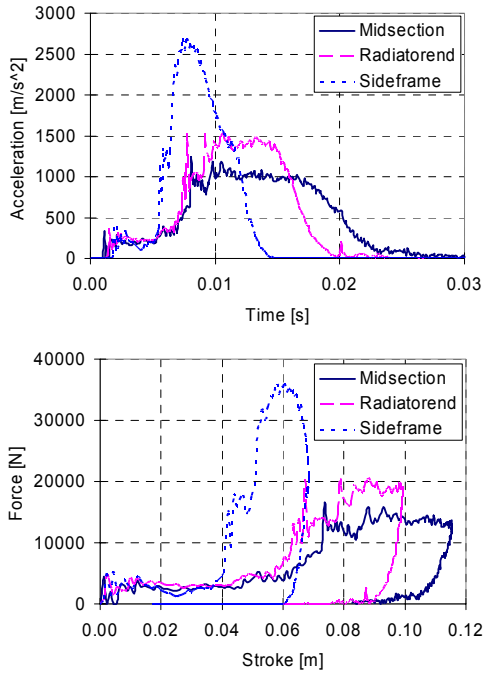

Figure 25. FE simulations of rigid legform to bumper impacts at three locations: acceleration-time (top) and contact force versus stroke (bottom).

The force-deflection curves from Figure 25 are filtered and implemented as contact stiffness characteristics in the vehicle model. Validation simulations are performed with the multi-body vehicle model and a rigid legform impactor. Results are shown in Figure 26 and resemble the FE data. No validation is performed for the area outside the side-frame, and hence the stiffness curve for the midsection is implemented there.

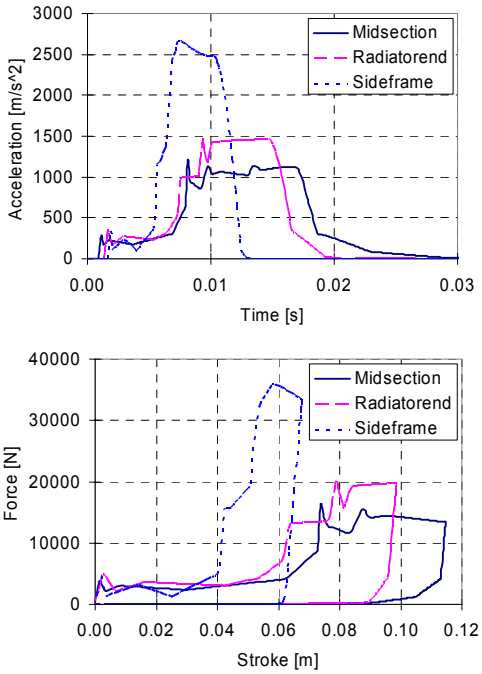

Figure 26. Validation of multi-body vehicle model bumper with rigid legform impacts at three locations: acceleration-time (top) and contact force versus stroke (bottom).

Hood edge For the hood edge the procedure followed to develop and validate the contact stiffness is similar. FE simulations are performed with rigid upper legform impactors, the stiffness characteristic is derived as before and MADYMO simulations are performed for validation. The three test setups are shown in Figure 27.

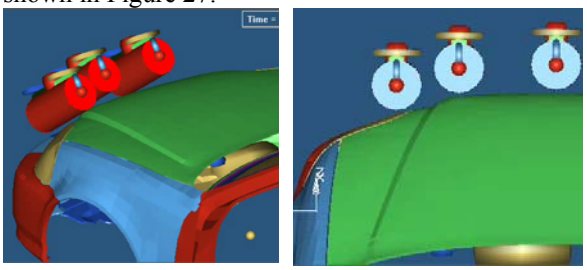

Figure 27. Test locations for upper legform to hood edge simulations as performed on the FE model of the vehicle and on the final multi-body model for validation.

The results from the FE simulation in Figure 28 show that the compliance of the three locations is comparable, since no local underlying structures are present directly under the hood edge. The validation with the multi-body vehicle model shows good correlation with the FE results, if we compare Figure 28 with Figure 29.

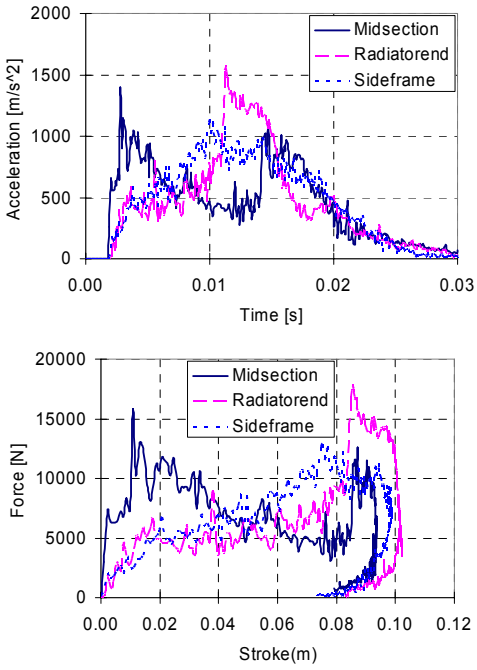

Figure 28. FE simulations of rigid upper legform impact to hood edge at three locations: acceleration-time (top) and contact force versus stroke (bottom).

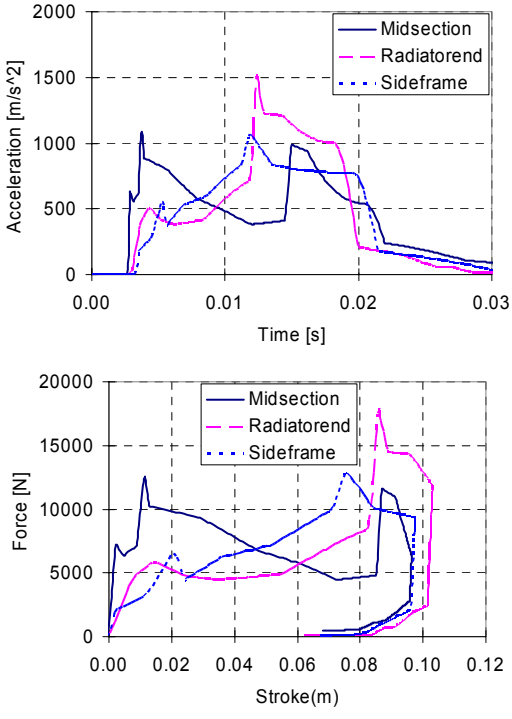

Figure 29. Validation of multi-body vehicle model hood edge with rigid upper legform impacts at three locations: acceleration-time (top) and contact force versus stroke (bottom).

Summary The currently developed model consists of a rigid finite element mesh that represents the front structure of the vehicle, ellipsoids that define structures directly under the hood and a multi-body framework that represents the vehicle and its suspension. The finite element mesh of the vehicle is subdivided in regions with different contact characteristics, as denoted in Table 1.

Table 1.

Contact Regions Of The Vehicle

Vehicle area	Contact Type
Windshield	4 regions, 4 contact stiffnesses
A-pillar	1 contact stiffness
Hood	1 contact stiffness + 12 ellipsoids with stiffness
Hood edge	3 regions, 3 contact stiffnesses
Bumper	3 regions, 3 contact stiffnesses

Mathematical Human Model

The current version of the MADYMO human pedestrian model (TNO 2001a) exists in 5 anthropometries; a 3-year-old and a 6-year-old child, a 5th percentile female, a 50th percentile male and a 95th percentile male all shown in Figure 30. The child anthropometries are based on the Q child dummy specifications (Ratingen 1997) whereas the adult anthropometries are based on the Western European population 8-70 years of age in 1984 (RAMSIS 1997). In addition, using the scaling module MADYSCALE, a model can be created of any anthropometry, of any age, based on 35 characteristic anthropometric parameters from the GEBOD population (TNO 2001b). The scaling accounts for geometry, mass and inertia, joint characteristics, ellipsoids and contact characteristics, force models, fracture levels, sensor locations and reference lengths based on dimensional scaling. The model consists of 52 rigid bodies, organized in 7 configuration branches, with an outer surface described by 64 ellipsoids and 2 planes. Stiffness characteristics are lumped into kinematic joints of various types (Figure 31) and the bending and fracture characteristics of the long bones of the lower extremity are represented by three frangible joints in the thigh and three in the leg. Contact properties of the human body are represented by ellipsoid contact models. The components shoulder, thorax, abdomen, pelvis and lower extremities have been validated for lateral impact against Post Mortem Human Subject (PMHS) tests (Kajzer 1990, Yang 1995, Kajzer 1993, Roberts 1991, ISO-N455 1996). Furthermore the model is validated against 8 full scale car to human impacts at speeds ranging from 25 to 39 km/h (Ishikawa 1993, Yang 2000).

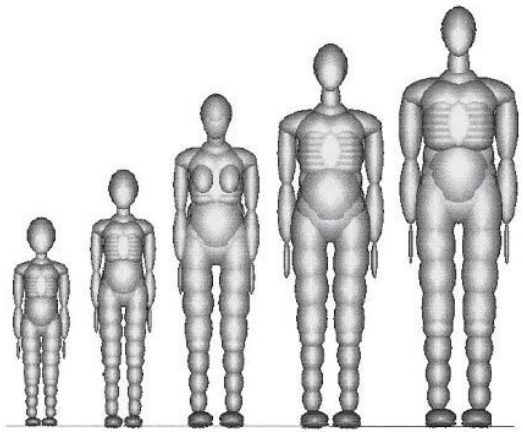

Figure 30. Overview of 5 anthropometries of MADYMO human pedestrian multi-body models. From left to right: 3-year old child, 6-year-old child, European 5th percentile female, European 50th percentile male and European 95th percentile male (TNO 2001a).

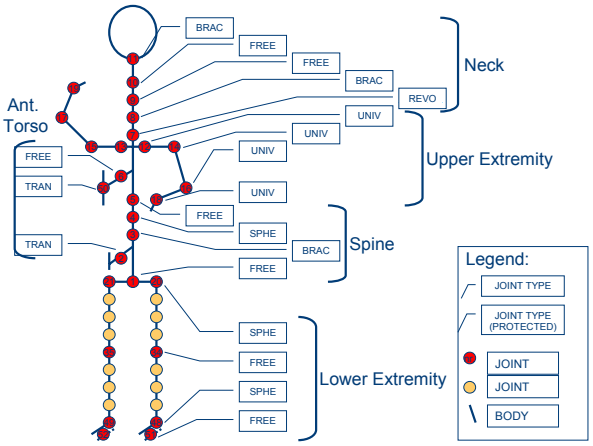

Figure 31. Overview of joints and bodies of the MADYMO human pedestrian model. Joint types are BRAC (bracket), TRAN (1 translational DOF), REVO, (1 rotational DOF), UNIV (2 rotational DOF), SPHE (3 rotational DOF) and FREE (6 DOF).

For this study the human models have been improved to provide more output signals for more injury criteria and to enable a better contact interaction with the facet mesh of the vehicle. All output signals of importance for injury prediction of pedestrian injuries are denoted in Appendix Table 5 for an American 50th percentile male. The injury reference values are denoted in the table as well. As a result, in the following, all injury criteria are presented as a percentage of the injury reference value.

MADYMO's contact algorithm for contact between an ellipsoid (e.g. the pedestrian's head) and a rigid finite element mesh (e.g. the windshield of the vehicle) is such that a contact force is generated from the windshield surface towards the center of the ellipsoid. This is shown in the diagram in Figure 32.

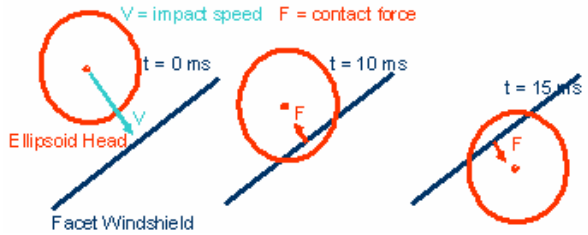

Figure 32. Diagram of the MADYMO contact algorithm for contact between an ellipsoid and a rigid finite element surface.

The ellipsoid head impacts the facet windshield at time = 0 ms, during which a contact force is applied to the head by the windshield. This force is directed from the windshield towards the center of the head ellipsoid. After 10 ms this contact force is directed so that the head is correctly pushed out of the windshield. At high impact speeds and low stiffness, the head can penetrate deeper. The schematic at time = 15 ms shows that the center of the head has penetrated the windshield to such an extent that the contact force is inverted. As a result, the contact force will push the head out towards the inside of the windshield. This instability is prevented by defining a rigid finite element mesh around the head. A different contact algorithm is then applied, which always generates the contact force in the correct direction. This problem occurs with head-windshield, hand-hood and knee-bumper contacts and necessitates the development of meshes for knees and hands as well.

REAL WORLD CRASH RECONSTRUCTION

Two cases are selected from the PCDS database based on the occurrence of severe injuries AIS (Abbreviated Injury Scale) 3 or more and on the case vehicle being the modeled small family car. In the following the two cases will be referred to as 50th male and stocky female, based on the anthropometries of the two case subjects.

Case Description And Model Setup

The data in Table 2 is retrieved from the respective PCDS case reports (PCDS 1996a, PCDS 1996b). One case subject is a near 50th percentile male, whereas the second case subject is a somewhat stocky adult female. Based on gender, height and weight a representative model is created for the latter subject using the MADYSCALE utility.

Table 2.

Case subject model setup data

	Case 50th M	Case stocky F
Age	35 years	18 years
Height	1.75 m	1.65 m
Weight	79 kg	104 kg
Struck on	Right	Front
Stance	Walking fast, right foot forward	Standing still, facing vehicle
Other	Holding lunchbox and thermos	BAC 0.04, drugs

The vehicles were the same model and were traveling at unknown speed in a straight line on a dry paved road in both cases. Based on skid marks, the speed of the vehicle at the point of impact with the 50th male pedestrian was estimated at 69 km/h, while throw-distance relationships (Bhalla 2002) provide a raw estimate of 55 km/h for the stocky female. The position of the subjects relative to the vehicles is based on points of first contact with the vehicle on the bumper. For the 50th male case contact points are near the midsection of the vehicle and along the latitude of the sidebeam (Figure 33). Figure 34 shows that the position of the stocky female relative to the vehicle was direct on the midsection.

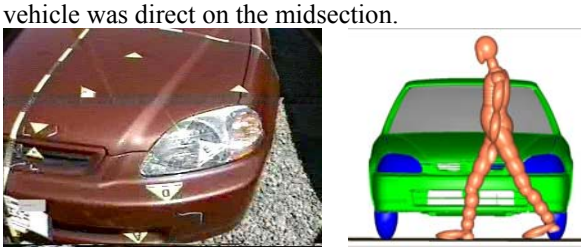

Figure 33. Photograph of case vehicle (PCDS 1996a) (left) and initial setup of pedestrian relative to vehicle (right) for the 50th male case. Contact points are shown with white triangles.

Figure 34. Photograph of case vehicle (PCDS 1996b) (left) and initial setup of pedestrian relative to vehicle (right) for the stocky female case. Contact points are shown with white triangles.

Simulations are performed at impact speeds ranging from 40 km/h to 75 km/h. It is assumed that both vehicles were braking at the time of impact, which is implemented in the model as a constant deceleration of 0.7 g. Other parameter variations consist of a rotation of the subject with 10° around its longitudinal axis, a different position of the arms for the stocky female and a posture where the 50th male is leaning backward. The latter is thought to replicate fast walking with an attempt to stop. A total number of 6 simulations are performed per case, each of which took approximately 30 minutes of CPU time on a Pentium III 1000 MHz PC with MADYMO v6.0.1 for 200 ms of simulation time.

Contact Points and Kinematics

One of the most important goals of the developed models is to be able to replicate the correct kinematics of the pedestrian relative to the vehicle. This can be achieved by comparing the kinematics of the models with the contact points on the case vehicles. Hence, two simulations remain as the most plausible based on the validity of the developed models and the accuracy of the PCDS case reports.

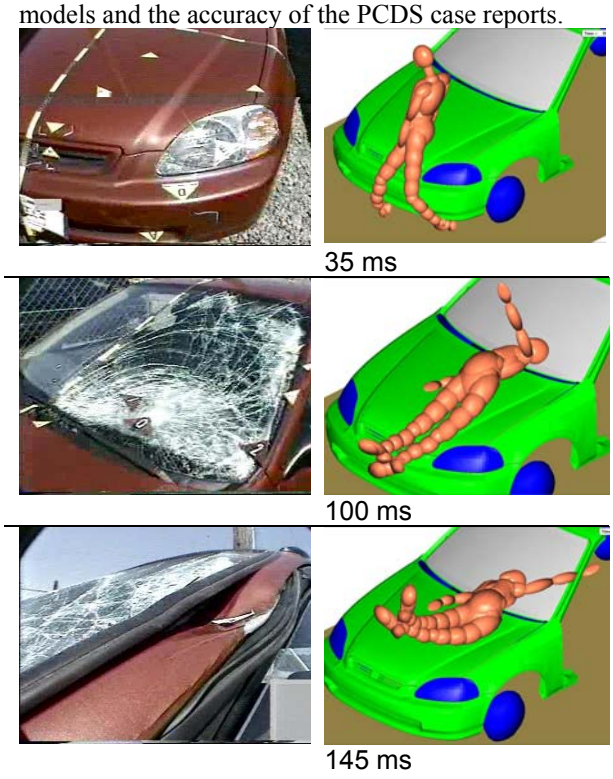

Figure 35. Photograph of case vehicle (PCDS 1996a) (left) and model kinematics (right) at time of impact with bumper, windshield and a-pillar for the 50th male case.

The contact points on the bumper obviously match those of the PCDS case since the human model is positioned relative to the vehicle based on those contact points. For both cases, contact marks on the hood consist of scuffs that may be caused by thorax, hip or upper extremity strikes. The behavior of the

arms is highly unpredictable due to a lack of information in the PCDS case reports on this and due to the free swinging and complex motion of the arms. Therefore, the markings on the hood merely indicate a direction of motion of the body as a whole. Parameter variations show that the location of impact of the head with the windshield is a function of the speed of impact. As speed increases, the head impacts the windshield at higher locations. Iterative simulations show that head to windshield impact locations match up if the simulations are performed with the initial positions shown in Figure 33 and Figure 34 at a speed of 65 km/h for the 50th male and at 55 km/h for the stocky female. Figure 35 and Figure 36 compare the contact points of the case vehicles with the model kinematics. The simulations show that head impact points match up with the windshield dents, while the left hand of the 50th male pedestrian impacts the a-pillar right at the location of the dent.

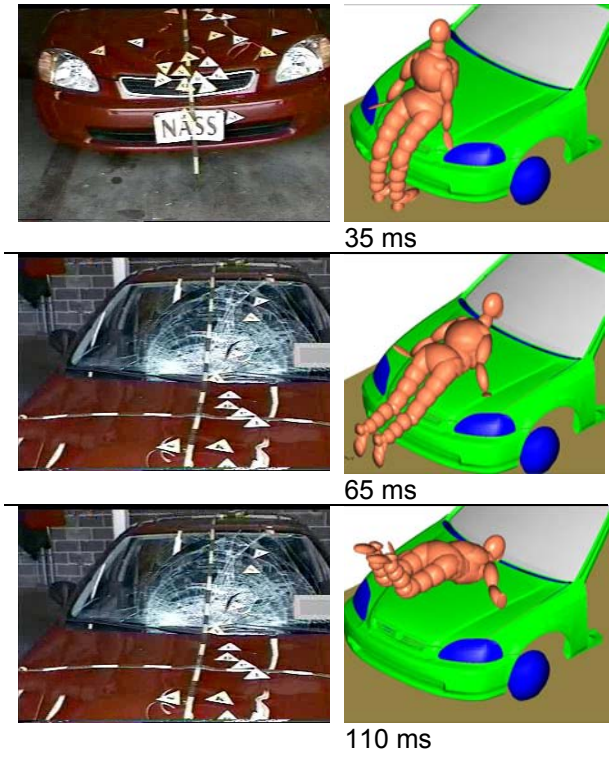

Figure 36. Photograph of case vehicle (PCDS 1996b) (left) and model kinematics (right) at time of impact with bumper and hood edge, hood and windshield for the stocky female case.

Injury Outcome and Prediction

The injury outcome is compared to the values that serve as injury predictors in the model for the specific injury types. Each case will be discussed separately

50th Male Case In Table 3 the various injuries are shown and compared to relative injury reference values obtained from the case reconstruction simulation. The orbital rim fracture on the left side corresponds to the high HIC value in the model, but in the kinematics of the simulations a contact of the left side of the face with the vehicle does not occur. It is anticipated that the orbital rim fracture might have been caused by the a-pillar impact, but the simulation does not predict this. No good shoulder injury predictor is available in the model, but TTI predicts high lateral acceleration in the upper torso, which might correlate with high shoulder loads.

Table 3.

Injury Outcome Compared To Model Injury Prediction For 50th Male Case

Injury of case subject	AIS	
Injury predictor from model		rIRV[%]
Orbital rim fracture L	2	
Head Injury Criterion (HIC)		2955
Resultant head angular acceleration		10889
Clavicle fracture L	2	
Thoracic Trauma Index (TTI)		91
ACL avulsion R	2	
Knee shear displacement R		37
Knee bending angle R		140
Knee dislocation L	2	
ACL rupture L	2	
PCL rupture L	3	
Popliteal tendon disruption L	2	
Knee shear displacement L		73
Knee bending angle L		188
Comminuted proximal tibia / fibula fracture R	3	
Upper tibia axial force R		132
Upper tibia bending moment R		42
Medial tibia plateau corner fracture L	3	
Upper tibia axial force L		150
Upper tibia bending moment L		14
Medial malleolus fracture R	1	
Ankle inversion/eversion angle		137

rIRV = relative Injury Reference Value (100% = IRV)
R = right, L = left, AIS = Abbreviated Injury Scale
ACL = anterior collateral ligament
PCL = posterior collateral ligament

The knee joints of both right and left lower extremities are severely damaged. The model predicts a bending angle above the injury tolerance and a shear displacement value below the injury tolerance. This is in correspondence with Bhalla's (2003) findings that shear displacement is not a good

predictor of knee injury. However, the impact is so severe that both left and right proximal tibia's are fractured. The model prediction shows a high axial force in the upper tibia, but a bending moment below the injury tolerance. The malleolar fracture in the right limb is predicted by an inversion/eversion angle above its limit.

Stocky Female Case Table 4 shows injury outcome from the hospital records with the relative injury reference values for the stocky female case.

Table 4.

Injury Outcome Compared To Model Injury Prediction For Stocky Female Case

Injury of case subject	AIS	
Injury predictor from model		rIRV[%]
Subdural brain hemorrhage	4	
Cerebral contusions, both lobes	3	
Subarachnoid cerebral + cerebellar hemorrhage	3	
Intraventricular hemorrhage	4	
Head Injury Criterion (HIC)		1121
Resultant head angular acceleration		1077
Atlanto occipital joint fracture dislocation	6	
Spinal cord transection below medulla oblongata	-	
Neck Injury Predictor (N_{ij}) Tens. Ext.		277
Neck Injury Predictor (N_{ij}) Tens. Flex.		38
Neck Injury Predictor (N_{ij}) Comp. Flex.		69
Upper neck axial force		144
Upper neck shear force		583
Kidney laceration L	2	
Thorax lateral displacement		80
Res. Lower torso acceleration		408

rIRV = relative Injury Reference Value (100% = IRV)

The patient died from an atlanto-occipital joint fracture dislocation. This injury is predicted by various high neck loads or N_{ij}, which is a combined criterion for axial load and bending. Judging from N_{ij} values, the injury mechanism appears to be a tension extension of the head relative to the body, which is plausible taking into account the body kinematics. Besides the high N_{ij}, also the shear force measured in the upper neck was five times higher than the injury reference value. The kidney laceration is an abdominal injury, for which the only predictor is lower torso acceleration which exceeded the injury tolerance value. Lateral displacement of the thorax also provides an indication for high compression in the abdomen. The value of 80% is just below the injury tolerance.

DISCUSSION

In this study, a detailed MADYMO vehicle model is developed in a simplified manner. The detail of the model is reflected by the outer mesh of the vehicle and the localized contact stiffness characteristics. This is a fairly simple and rapid method compared to a full finite element vehicle model with material models. However, the currently developed method is fairly detailed compared to multi-body ellipsoid models that have been used in previous studies. Those models contain less detail and less diverse stiffness characteristics.

This study shows that besides a correct estimate of crash parameters, such as impact speed and pedestrian anthropometry, detailed descriptions of the vehicle geometry and stiffness have a great influence on the model response. Simulations show that the geometry of the car largely determines the wrap distance of the pedestrian and, hence, determines where on the vehicle the various body types impact. Combined with the localized contact stiffness characteristics, the location of impact of a body part is of great influence on the injury outcome, due to varying contact characteristics over the vehicle. A 5 cm decrease in the total height of the vehicle causes the head to impact approximately 5 cm higher on the windshield and the corresponding much more compliant windshield region. This also demonstrates the importance of applying suspension to the vehicle model. An additional effect of correct contact characteristics is the energy absorbing capability of the various structures. A contact with an appropriate hysteresis model will absorb some of the impact energy of the pedestrian. This has an effect on the kinematics of the upper body, which will influence the impact location of head and thorax and therefore also the corresponding injury prediction.

The anthropometry of the human pedestrian model is of great importance in pedestrian crash reconstruction. For example, a factor like knee height relative to bumper height has an influence on the injury response due to bumper contact. The knee joint is sensitive to impact location of the bumper. The bumper of a small family car impacts above the knee joint of a small adult, while the same vehicle impacts below the knee joint of a taller person, resulting in a completely changed injury mechanism. The same holds for the head impact location, which is largely determined by the average height of the subject. For future crash reconstructions, models are available for 5 typical anthropometries. If a different anthropometry is required, it is possible to scale a full

human pedestrian model, including inertial and joint properties.

Injury tolerance values are provided for an American 50th percentile male in Appendix Table 5. Scaling of injury tolerance values to different anthropometries and age groups has been performed based on geometric variability (TNO 2001a). In addition, there is a large gradient in material characteristics of biological tissues between children, middle-aged people and the elderly. Therefore, for future crash reconstruction, injury criteria need to be scaled for the age-dependency of material characteristics, especially for children and the elderly. The latter does not apply for the two case subjects in this study, since they were both middle-aged adults. Nevertheless, the injury tolerance levels for the stocky female are doubtlessly different from a 50th percentile male, but no information is currently available on the influence of a stocky anthropometry on the scaling of injury criteria. Therefore, the injury tolerance values for the stocky female are adopted from the 50th percentile male as denoted in Appendix Table 5.

The MADYMO human pedestrian model is a fairly detailed and numerically fast tool to evaluate injury mechanisms in impacts to vehicles. The multiple segments allow for localized injury prediction at various locations in the lower extremities, the torso, the spine and the neck. Nevertheless, no validated injury predictor is implemented for pelvic, abdominal and shoulder injuries. In the current model, the contact force of the shoulder, abdomen and pelvis with the vehicle is applied for injury prediction, while an internal force or displacement criterion is preferable. The knee joint of the current model is adopted from EEVC WG17 legform impact results. However, the biomechanical foundations of this knee are questionable and as a result an improvement to the knee model is recommended based on cadaveric tests (Konosu 2001, Takahashi 2001, Bhalla 2003). Although the human pedestrian model is omni-directional, it is only validated for a lateral impact in a walking stance at speeds up to 40 km/h. In this study the model has been applied at higher velocities, where the generation of a facet mesh around various body parts solved for problems occurring due to high penetrations. Also, the model has been applied in a facing position, where again correct kinematics and injury patterns were predicted.

The numerical simplifications that are made by implementing the vehicle and pedestrian in a multi-body description lead to limitations of the application. In reality, as the head impacts the windshield, both structures deform. With two deforming structures, the contact area is slightly different than with two rigid structures with a contact interface. The influence of this can currently not be quantified, but it is only of influence on large structures with relatively large deformations, such as hood and windshield. Another numerical artifact is that the MADYMO contact algorithm does not allow for a combined stiffness model. Therefore, in the current model the contact stiffness of the human model is ignored. This is a valid assumption if the human structure is much stiffer than the vehicle, which is true for head and knee, but not for abdomen and thigh areas. As a result, the injury outcome from the model has to be interpreted with caution for the more compliant body regions, but is presumably unaffected for the stiffer body regions. In future studies, combined contact characteristics need to be appointed for every contact interaction between a body part and a vehicle region.

CONCLUSIONS

In summary, the multi-body techniques developed in this paper permit the following advances in pedestrian-impact simulations:

- **Detailed geometric modeling** of the vehicle front by using a facet surface mesh representation
- **Accurate vehicle stiffness functions** developed and validated by comparison with EEVC sub-system impactor test results
- **Incorporation of stiffness maps** by subdividing the vehicle parts (hood, bumper, etc) into regions of varying stiffness
- **Inclusion of a vehicle suspension model** allows accurate modeling of vehicle pitching during the pedestrian impact phase.
- **Application of a scalable human model with advanced injury criteria** predicts kinematics and injury outcome

The accuracy of the vehicle models approaches that of finite element models at a fraction of the computational time. Thus, making it possible to perform parametric studies by running a large number of simulations.

The use of the models is demonstrated by application to the reconstruction of two real world pedestrian crashes. Iterative simulations are performed until a good match is obtained with vehicle damage and pedestrian injuries using the advanced pedestrian injury criteria. Thus, an improved understanding into the sequence of events and injury mechanisms in car-pedestrian impacts is gained.

ACKNOWLEDGEMENTS

The authors would like to thank Ronald de Lange of TNO Automotive, Crash Safety Center, Delft, The Netherlands for sharing his expertise on pedestrian human modeling with us and for his technical support on applying and improving the MADYMO human pedestrian models.

REFERENCES

Bhalla, K., Montazemi, P., Crandall, J., Yang, J., Liu, X., Dokko, Y., Takahashi, Y., Kikuchi, Y., Longhitano, D., "Vehicle Impact Velocity Prediction from Pedestrian Throw Distance: Trade-Offs between Throw Formulae, Crash Simulators, and Detailed Multi-Body Modeling", Proc. Int. IRCOBI Conf. Biomechanics of Impact, September 18-20 2002, Munich, Germany, 2002

Bhalla, K., Bose, D., Madeley, J., Kerrigan, J., Crandall, J., Longhitano, D., Takahashi, Y., "Evaluation of the Response of Mechanical Pedestrian Knee Joint Impactors in Bending and Shear Loading", Proceedings of the 18th International Conference on the Enhanced Safety of Vehicles (ESV), Nagoya, Japan, May 2003

Chidester, A., Isenberg, R., "Final Report – The Pedestrian Crash Data Study", Proceedings of the 17th International Conference on the Enhanced Safety of Vehicles (ESV), Amsterdam, The Netherlands, June 2001

Coley, G., Lange, R. de, Oliveira, P. de, Neal-Sturgess, C., Happee, R., "Pedestrian Human Body Validation Using Detailed Real-World Accidents", Proc. Int. IRCOBI Conf. Biomechanics of Impact, October 10-12 2001, Isle of Man, United Kingdom, 2001

Crandall, J., Funk, J., Rudd, R., Tourret, L., "The Tibia Index: a Step in the Right Direction", Proceedings of the Toyota International Symposium on Human Life Support Biomechanics, Nagoya, Japan, 1999

DeSantis Klinich, K., Saul, R., Auguste, G., Backaitis, S., Kleinberger, M., "Techniques for Developing Child Dummy Protection Reference Values", NHTSA Child Injury Protection Team, Event Report, 1996

Eppinger, R., Sun, E., Kuppa, S., Saul, R., "Supplement: Development of the Improved Injury Criteria for the Assessment of Advanced Automotive Restraint Systems – II", 2000, http://www-nrd.nhtsa.dot.gov/pdf/nrd-11/airbags/finalrule_all.pdf (accessed November 21 2002).

European Enhanced Vehicle-safety Committee, "EEVC Working Group 10 Report: Proposals for Methods to Evaluate Pedestrian Protection for Cars", November 1994

European Enhanced Vehicle-safety Committee, "EEVC Working Group 17 Report: Improved Test Methods to Evaluate Pedestrian Protection Afforded by Passenger Cars", December 1998 http://www.eevc.org/publicdocs/WG17_Improved_test_methods.pdf (accessed February 20 2003)

Federal Motor Vehicle Safety Standards, "Standard No. 208; Occupant Crash Protection", US Department of Transportation National Highway Traffic Safety Administration, http://www.access.gpo.gov/nara/cfr/waisidx_00/49cfr571_00.html (accessed February 20 2003).

Federal Motor Vehicle Safety Standards, "Standard No. 214; Side Impact Protection", US Department of Transportation National Highway Traffic Safety Administration, http://www.access.gpo.gov/nara/cfr/waisidx_00/49cfr571_00.html (accessed February 20 2003).

Funk, J., Srinivasan, S., Crandall, J., Khewpong, N., Eppinger, R., Jaffredo, A., Potier, P., Petit, P., "The Effects of Axial Preload and Dorsiflexion on the Tolerance of the Ankle/Subtalar Joint to Dynamic Inversion and Eversion" In Stapp Car Crash Journal 46, 2002

Ishikawa, H., Kajzer, J., Schroeder, G., "Computer Simulation of Impact Response of the Human Body in Car-Pedestrian Accidents, SAE Paper No.933129, 37th Stapp Car Crash Conference, November 1993

ISO-N455, "Road Vehicle – Anthropomorphic Side Impact Dummy – Lateral Response Requirements to Assess the Biofidelity of the Dummy ", ISO/TC22/SC12/WG5, Document N455, Revision 2, May 1996

Jarrett, K., Saul, R., "Pedstrian Injury – Analysis of the PCDS Field Collision Data", Proceedings of the 16th International Conference on the Enhanced Safety of Vehicles (ESV), Windsor, Canada, June 1998

Kajzer, J., Cavallero, C., Ghanouchi, S., C., Bonnoit, J., Ghorbel, A., "Response of the Knee Joint in Lateral Impact : Effect of Shearing Loads", Proc. Int. IRCOBI Conf. Biomechanics of Impact, September 12-14 1990, Bron, France, 1990

Kajzer, J., Cavallero, C., Bonnoit, J., Morjane, A., "Response of the Knee Joint in Lateral Impact : Effect of Bending Moment", Proc. Int. IRCOBI Conf. Biomechanics of Impact, September 8-10 1993, Eindhoven, The Netherlands, 1993

Kajzer, J., Schroeder, G., Ishikawa, H., Matsui, Y., Bosch, U., "Shearing and Bending Effects at the Knee Joint at High Speed Lateral Loading" In Proceedings of the 41st Stapp Car Crash Conference, 1997

Konosu, A., Ishikawa, H., Tanahashi, M., "Reconsideration of Injury Criteria for Pedestrian Subsystem Legform Test - Problems of Rigid Legform Impactor", Proceedings of the 17th International Conference on the Enhanced Safety of Vehicles (ESV), Amsterdam, The Netherlands, June 2001

Liu, X., Yang, J., Lövsund, P., "A Study of Influences of Vehicle Speed and Front Structure on Pedestrian Impact Responses using Mathematical Models", Traffic Injury Prevention, 2002, 3(1): 31-42, 2002a

Liu, X., Yang, J., "Development of Child Pedestrian Mathematical Models and Evaluation with Accident Reconstruction", Traffic Injury Prevention, 2002, 3(4): 321-329, 2002b

Liu, X., Yang, J., "Effects of Vehicle Impact Velocity and Front-End Structures on Dynamic Responses of Child Pedestrians", Proc. Int. IRCOBI Conf. Biomechanics of Impact, September 18-20 2002, Munich, Germany, 2002c

Lund, A., "Recommended Procedures for Evaluating Occupant Injury Risk from Deploying Side Airbags", The Side Airbag Out-of-Position Injury Technical Working Group, 2000

Mackay, M., "Folklore and Science in Traffic Safety: Some New Directions", In Injury Prevention and Control, Editors: Mohan, D. & Tiwari, G., London, United Kingdom: Taylor & Francis, pp. 89-98, 2000

Maeno, T., Hasegawa, J., "Development of a Finite Element Model of the Total Human Model for Safety (THUMS) and Application to Car-Pedestrian Impacts", Proceedings of the 17th International Conference on the Enhanced Safety of Vehicles (ESV), Amsterdam, The Netherlands, June 2001

Mertz, H., Patrick, L., "Strength and Response of the Human Neck" In Proceedings of the 15th Stapp Car Crash Conference, 1971

Miltner, E., Kallieris, D., "Quasistatische und Dynamische Biegebelastung des Kindlichen Oberschenkels zur Erzeugung einer Femurfraktur. Zeitschrift für Rechtsmedizin, In German, 102(8), pp. 535-544, 1989

Mizuno, K., Kajzer, J., "Head Injuries in Vehicle-Pedestrian Impact", SAE Paper No. 2000-01-0157, Society of Automotive Engineers, Warrendale, PA, 2000

NHTSA, "Traffic Safety Facts 2001: A Compilation of Motor Vehicle Crash Data from the Fatality Analysis Reporting System and the General Estimates System", Washington, DC: US Department of Transportation National Highway Traffic Safety Administration, 2001, http://www-nrd.nhtsa.dot.gov/pdf/nrd-30/NCSA/TSFAnn/TSF2001.pdf (accessed February 20 2003)

Nyquist, G., "Injury Tolerance Characteristics of the Adult Human Lower Extremities under Static and Dynamic Loading" SAE Paper No. 861925, Society of Automotive Engineers, Warrendale, PA, 1986

Ommaya, A., "Mechanisms and Preventive Management of Head Injuries: a Paradigm for Injury Control", The George G. Snively Memorial Lecture, In Proceedings of the 38th annual Association for the Advancement of Automotive Medicine (AAAM) Conference, Seattle, Washington, Separate Article, 1988

Otte, D., Pohlemann, T., "Analysis and Load Assessment of Secondary Impact to Adult Pedestrians After Car Collisions on Roads", Proceedings of the 17th International Conference on the Enhanced Safety of Vehicles (ESV), Amsterdam, The Netherlands, June 2001

PCDS, "Pedestrian Crash Data Study Case Report, (Case Number Confidential)", US Department of Transportation National Highway Traffic Safety Administration, 1996a

PCDS, “Pedestrian Crash Data Study Case Report, (Case Number Confidential)”, US Department of Transportation National Highway Traffic Safety Administration, 1996b

Ratingen, M., Twisk, D., Schrooten, M., Beusenberg, M., Barnes, A., Platten, G., “Biomechanically Based Design and Performance Targets for a 3-Year-Old-Child Crash Dummy for Front and Side Impact”, SAE Paper No. 973316, Society of Automotive Engineers, Warrendale, PA, 2000

RAMSIS, “RAMSIS Manual Version 3.1”, Tecmath Gmbh, Kaiserlautern, Germany, 1997

Roberts, A., “Test Procedures for Defining Biofidelity Targets for Lateral Impact Test Dummies”, Report of EEVC WG09, Proceedings of the 13th International Conference on the Enhanced Safety of Vehicles (ESV), Paris, France, 1991

Schreiber, P., Crandall, J., Micek, T., Hurwitz, S., Nusholtz, G., “Static and Dynamic Bending Strength of the Leg”, Proc. Int. IRCOBI Conf. Biomechanics of Impact, September 24-26 1997, Hannover, Germany, 1997

.

Schuster, P., Chou, C., Prasad, P., Jayaraman, G., “Development and Validation of a Pedestrian Lower Limb Non-Linear 3-D Finite Element Model”, 44th Stapp Car Crash Conference, Paper No. 2000-01-SC21, November 2000

Takahashi, Y., Kikuchi, Y., Konosu, A., Ishikawa, H., “Development and Validation of the Finite Element Model for the Human Lower Limb of Pedestrians”, 44th Stapp Car Crash Conference, Paper No. 2000-01-SC22, November 2000

Takahashi, Y., Kikuchi, Y., “Biofidelity of Test Devices and Validity of Injury Criteria for Evaluating Knee Injuries to Pedestrians”, Proceedings of the 17th International Conference on the Enhanced Safety of Vehicles (ESV), Amsterdam, The Netherlands, June 2001

TNO, “MADYMO Human Models Manual, Version 6.0”, TNO Automotive, Delft, The Netherlands, May 2001a

TNO, “MADYMO Utilities Manual, Version 6.0”, TNO Automotive, Delft, The Netherlands, May 2001b

Viano, D., Lau, I., Asbury, C., King, A., Begeman, P., “Biomechanics of the Human Chest, Abdomen and Pelvis in Lateral Impact”, In Accident, Analysis and Prevention, 21(6), pp. 553-574, 1989

Wijk, J. van, Wismans, J., Wittebrood, L., “MADYMO Pedestrian Simulations”, SAE Paper No. 830060, Society of Automotive Engineers, Warrendale, PA, 1983

World Bank Group, “Road Safety”, 2003, http://www.worldbank.org/html/fpd/transport/roads/safety.htm (accessed February 20 2003)

Yang, J., Lövsund, P., Cavallero, C., Bonnoit, J., “A Human-Body 3D Mathematical Model for Simulation of Car-Pedestrian Impacts”, Journal of Crash Prevention and Injury Control, 2000, 2(2): 131-149, 2000

Yang, J., Kajzer, J., Cavallero, C., Bonnoit, J., “Computer Simulation of Shearing and Bending Response of the Knee Joint to a Lateral Impact”, 39th Stapp Car Crash Conference, 1995

Appendix Table 5. Injury Criteria and Levels for American 50th Percentile Male

Body Region	Injury Criterion	Value	Injury Level	Source
Head	HIC [value]	1000	Low probability of serious injury	VRTC (as cited for 50th % in the first row of Table 34 in DeSantis Klinich et al. (1996))
	HIC [time window]	15 ms		
	Max linear acceleration (g)	85		
	Angular velocity change (rad/s) and angular acceleration (rad/s^2)	$\omega\Delta > 30$ $\alpha p < 3000$	AIS 3	Ommaya (1988)
Neck	Fshear (N)	845	Tolerance level	Mertz and Patrick (1971)
	Ftension (N)	3290	Dummy IARVs (an Nij value of 1 corresponds to a 15% risk of AIS 3+ neck injury)	Eppinger et al. (2000) Lund (2000)
	Fcompression (N)	4000		
	Nij - Ftens-int (N)	6160		
	Nij – Fcomp-int (N)	6160		
	Nij - Mx-int (Nm)	216		
Chest	Peak lateral acc. of T8 (g)	45.2	25% probability of AIS 4+	Viano et al. (1989)
	Peak lateral acc. of T12 (g)	31.6		
	TTI(d) (g)	85	Dummy IARV	FMVSS 214 (2003)
	(VC)max (m/s) (to whole thorax)	1.47	25% probability of AIS 4+	Viano et al. (1989)
	Compression (%) (to whole thorax)	38.4		
Abdomen	Force (kN)	7.48	25% probability of AIS 4+	Viano et al. (1989)
Pelvis	Force (kN)	7.98	25% probability of fracture	Cavanaugh et al. (1990)
Femur	Axial Force Fz (kN)	10	Injury threshold	FMVSS 208 (2003)
	Anterior-Posterior Bending Moment Mx (Nm)	524	Fracture threshold	Messerer in Nyquist (1986), Schreiber et al. (1997), Miltner and Kallieris (1989)
	Lateral Bending Moment My (Nm)	524		
Tibia	Lateral acceleration (g)	150	40% risk for AIS 2+ lower leg fracture	EEVC WG 17 (1998)
	Axial Force Fz (kN)	10.4	Failure threshold	Messerer in Nyquist (1986)
	Tibia Index - Fcr (kN)	18.3	Onset of injury	Crandall et al. (1999)
	Tibia Index - Mcr (Nm)	450		
Knee	Bending Angle (degrees)	14.6	Injury threshold	Kajzer et al. (1997)
	Shear Displacement (mm)	16		
Ankle	Inversion/eversion angle (deg)	28	25% risk of injury	Funk et al. (2002)